ACS Synthetic Biology



pubs.acs.org/synthbio
Research Article

# Tunable T7 Promoter Orthogonality on T7RNAP for *cis*-Aconitate Decarboxylase Evolution via Base Editor and Screening from Itaconic Acid Biosensor

Wan-Wen Ting and I-Son Ng*

Cite This: *ACS Synth. Biol.* 2023, 12, 3020–3029
Read Online



**ABSTRACT:** The deaminase-fused T7 RNA polymerase (T7RNAP) presents a promising toolkit for *in vivo* target-specific enzyme evolution, offering the unique advantage of simultaneous DNA modification and screening. Previous studies have reported the mutation efficiency of base editors relying on different resources. In contrast, the mechanism underlying the T7RNAP/T7 system is well-understood. Therefore, this study aimed to establish a new platform, termed dT7-Muta, by tuning the binding efficiency between T7RNAP and the T7 promoter for gene mutagenesis. The strategy for proof-of-concept involves alterations in the fluorescence distribution through dT7-Muta and screening of the mutants via flow cytometry. The *cis*-aconitate decarboxylase from *Aspergillus terreus* (AtCadA) was evolved and screened via an itaconate-induced biosensor as proof-of-function of enzyme evolution. First, the degenerated codons were designed within the binding and initial region of T7 promoters (dT7s), including upstream (U), central (C), and downstream (D) regions. Three strength variants of dT7 promoter from each design, i.e., strong (S), medium (M), and weak (W), were used for evaluation. Mutation using dT7s of varying strength resulted in a broader fluorescence distribution in sfGFP mutants from the promoters CW and DS. On the other hand, broader fluorescence distribution was observed in the AtCadA mutants from the original promoter T7, UW, and DS, with the highest fluorescence and itaconic acid titer at 860 a.u. and 0.51 g/L, respectively. The present platform introduces a novel aspect of the deaminase-based mutagenesis, emphasizing the potential of altering the binding efficiency between T7RNAP and the T7 promoter for further efforts in enzyme evolution.

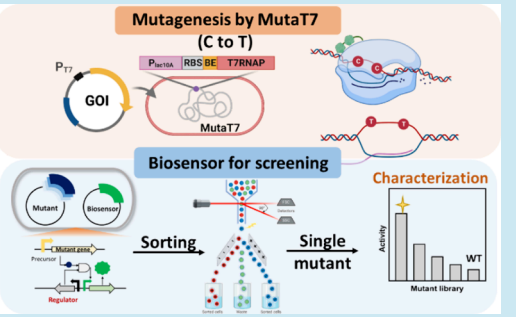


**KEYWORDS:** *directed evolution, biosensor-based screening, binding efficiency, T7 RNA polymerase (T7RNAP), cis-aconitate decarboxylase*

## INTRODUCTION

The emergence of sophisticated techniques in synthetic biology has expedited the transition from modifying the genetic elements to manipulating metabolic pathways for eco-friendly production of chemicals or pharmaceuticals.[1,2] Utilizing novel metabolite pathways from natural producers necessitates the discovery of enzyme systems with straightforward regulatory mechanisms in order to achieve optimal catalytic efficiency.[3] However, achieving maximum yield is hampered by factors such as low catalytic efficiency, feedback inhibition, or stringent reaction conditions.[4] To address these challenges, directed evolution is applied to facilitate protein engineering of enzymes via random or rational design strategies, with numerous cycles of design-build-test-learn to generate the desired superior variants.

Directed evolution is an essential pillar in modern protein engineering, propelling the rapid advancement of new biomolecules and biocatalysts.[5−7] While its prowess is well-recognized for improving the catalytic activity of individual enzymes,[8,9] the scope extends to refine the ligand selectivity of transcriptional regulators for biosensors,[10,11] or the modification of an entire metabolic pathway for chemical production.[12,13] Traditional gene modification relies on *in vitro* mutagenesis. However, the initial rounds of mutation and subsequent laborious screening of numerous mutants have limited the scope of obtaining variant pools, largely due to the inefficiency of DNA uptake. *In vivo* gene modification streamlines the process by synergistic mutagenesis and screening. Cytidine deaminase catalyzes the irreversible hydrolytic deamination of deoxycytidine (dC) to deoxyuridine (dU), which participates in the pyrimidine salvage pathway to maintain cellular pyrimidine supply.[14] During transcription, deoxyuridine (dU) is recognized as deoxythymidine (dT) and pairs with deoxyadenosine (dA) during DNA replication.[15]

**Received:** June 5, 2023
**Published:** September 26, 2023





https://doi.org/10.1021/acssynbio.3c00344
*ACS Synth. Biol.* 2023, 12, 3020−3029

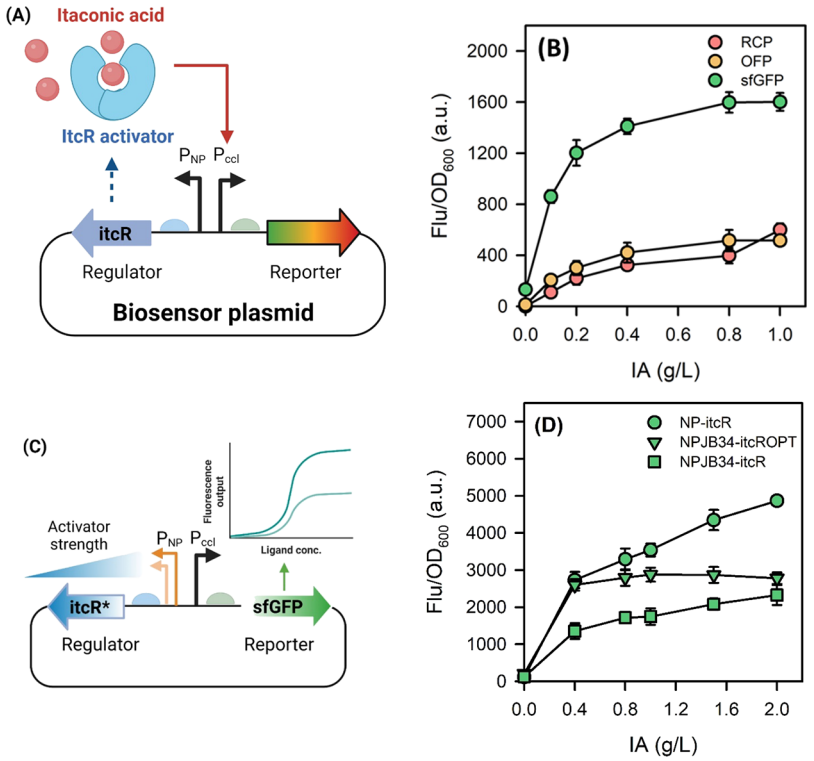


**Figure 1.** Establishment of itaconic acid biosensor for high-throughput screening. (A) Illustration of activator-based itaconic acid biosensor. (B) Different specific fluorescence intensities of the itaconic acid biosensor under different concentrations of itaconic acid from 0 to 1 g/L at 16 h. (C) Schematic diagram of tuning the biosensor by regulating the promoter strength and codon of regulator itcR. (D) Specific intensity of the three designs with different concentrations of itaconic acid from 0 to 2 g/L at 16 h. The NP-itcR used the native design of biosensor. NPJB34-itcR and NPJB34-itcROPT represent the insertion of $P_{J23100}$ with RBS B0034 downstream of $P_{NP}$ without and with codon optimization of regulator *itc*R, respectively.

Recent successes have showcased the collaborative prowess of deaminase with a target-specific enzyme for the evolution of target proteins. Among all of them, T7 RNA polymerase (T7RNAP) from bacteriophage, which is highly specific to the cognate promoter T7 during transcription, is the ideal candidate for enzyme evolution. The chromosome-based fusion of cytidine deaminase with T7RNAP, known as MutaT7, using rAPOBEC1 from rat (apolipoprotein B mRNA editing enzyme, catalytic polypeptide 1), demonstrated the feasibility of mutating dC to dT at a rate of 0.34 mutations/day/kbp.[16] On the other hand, the fusion of activation-induced cytidine deaminase (AID) with T7RNAP, i.e., T7 polymerase-driven continuous editing (TRACE), performed continuous mutation in human cell lines.[17] Furthermore, the cytidine deaminase from *Petromyzon marinus* (PmCDA1) elevated the mutation rate up to 4 mutations/day/kbp.[18] TadA, originally identified in *E. coli* as a tRNA editing enzyme, catalyzes the conversion of deoxyadenosine (dA) to deoxyinosine (dI), which was recognized as deoxyguanosine (dG) by the cellular machinery.[19] The evolved TadA-8e variant exhibited an enhanced activity ($k_{app}$) of up to 590-folds, resulting in a higher mutation efficiency but also a higher off-target rate.[20] A combination of cytidine deaminase and adenosine deaminase achieved alterations in all accessible base pairs, leading to approximately 6.7 bp substitutions within 80 h of *in vivo* mutagenesis.[21,22] Therefore, it is evident that the mutation rate is controlled by the base editor. However, the relationship between the T7RNAP-T7 promoter binding efficiency and mutation efficiency remains unexplored.

Apart from mutagenesis, high throughput screening is also essential to select variants with optimal parameters. Genetically encoded biosensors activated by specific metabolites have emerged as invaluable tools for the real-time monitoring of gene regulation during biobased chemical production. Employing transcription-factor-based biosensors has become a common strategy for quantitatively determining the levels of metabolite, facilitating high throughput screening and adaptive evolution based on the signal readout.[23−25] Itaconic acid (IA) is a value-added chemical and a building block for polymers. The synthesis of IA in *Aspergillus terreus* involves a two-step reaction mediated by aconitase (EC 4.2.1.3) and *cis*-aconitate decarboxylase (EC 4.1.1.6) with remarkable titers.[26] However, an imbalance in the catalytic velocity of the two participating enzymes was observed highlighting the reaction catalyzed by cis-aconitate decarboxylase as the rate-limiting step.[27]

Herein, we aimed to evolve the *cis*-aconitate decarboxylase from *Aspergillus terreus* (AtCadA) by employing the tunable cytidine-deaminase-fused T7RNAP (MutaT7), followed by screening using an IA biosensor. We systematically investigated the impact of factors including fluorescence reporters, activator quantity, and culture medium on the dynamic range of the IA-based screening system. Furthermore, we applied the degenerated oligos for the T7 promoter, referred to as dT7, to modulate the transcriptional rate of T7RNAP. The efficacy of the modulation was validated by assessing the fluorescence distribution of super folder green fluorescent protein (sfGFP) through fluorescence-activated cell sorter (FACS) analysis. For the proof-of-function demonstration, we exploited six reverse dT7 promoter variants to generate mutations in AtCadA and


https://doi.org/10.1021/acssynbio.3c00344
ACS Synth. Biol. 2023, 12, 3020−3029

screen the mutants via a high-throughput screening system based on the IA biosensor in an inefficient IA producing strain. This study has unveiled the relationship between the strength of the dT7 promoters and the resultant mutation efficiency, shedding light on this unexplored aspect for the first time.

## RESULT AND DISCUSSION

**Establishment of IA Biosensor.** The catabolism of IA existed in several bacteria, and the regulatory modules associated with *Yersinia pestis* and *Pseudomonas aeruginosa* have been characterized recently.[28] The sequential degradation of IA to pyruvate and acetyl-CoA is mediated by enzymes including itaconate CoA transferase (Ict), itaconyl-CoA hydratase (Ich), and citramalyl-CoA lyase (Ccl). Concurrently, an upstream LysR-type transcriptional regulator, ItcR, has been identified in the degradation operon.[29,30] Evaluating the response of on−off status in *E. coli* and *C. necator*, the biosensor design was based on itaconate-induced activator-based regulator ItcR and its corresponding promoter $P_{ccl}$ from *Yersinia pseudotuberculosis* (Figure 1A). To initiate the biosensor design, the fluorescence readout of superfolded GFP (sfGFP), orange fluorescence protein (OFP), and red chromoprotein (RCP) were characterized. Using LB medium with 0−1 g/L IA, the highest fluorescence recorded for sfGFP, RCP, and OFP were 1602, 599, and 515 a.u., respectively (Figure 1B). However, the dynamic range of sfGFP was only 12.2-fold. To augment the dynamic range of the biosensor, we engineered the activator by inserting an additional promoter and RBS upstream of *itc*R. Three designs were explored, including (1) the original NP-itcR, (2) NPJB34-itcR, with an insertion of $P_{J23100}$ and B0034 RBS, and (3) NPJB34-itcROPT, using a codon-optimized *itc*R (itcROPT) (Figure 1C). As a result, the dynamic range improved to 40.5-folds, 18.9-folds, and 13.2-folds for NP-itcR, NPJB34-itcR, and NPJB34-itcROPT, respectively, in M9 medium with IA concentrations in the range of 0 to 2 g/L as shown in Figure 1D.

The performance of the biosensor was assessed based on the specificity, sensitivity, dynamic range, detection range, and the response time.[30] A balance in the expression levels of the transcription factor and reporter gene significantly impacts signal output and place metabolic stress on strains.[31] Consequently, modification of promoters, transcription factors, and transcription factor binding sites have been illustrated to improve the biosensor signal. In a previous study, rational regulator engineering of tryptophan repressor resulted in a 10-fold improvement in dynamic range.[32] Furthermore, engineered promoters and RBS were applied to influence the expression of regulator[33,34] through machine learning, which enabled the prediction of dynamic range based on RBS strength.[35] Hence, the performance of NP-itcR was further evaluated using M9, M9Y, M9C3, and M9C3Y mediums. In this context, Y represented yeast extract as a rich nitrogen source, leading to higher biomass in M9Y and M9C3Y compared to that in M9 and M9C3, respectively (Figure 2A). On the other hand, an increase in IA titer slightly inhibited cell growth. The specific fluorescence reached 6000 and 4100 a.u. in M9Y and M9C3Y mediums, respectively, indicating the benefits of nitrogen source supplementation (Figure 2B). Given the higher fluorescence intensity in the M9-series medium comparing to M9C3-series medium, we further investigated the two-slope dosage curve using M9-series medium. The detection of lower IA dosages from 0 to 0.25 g/L in M9 and M9Y mediums attained a specific fluorescence

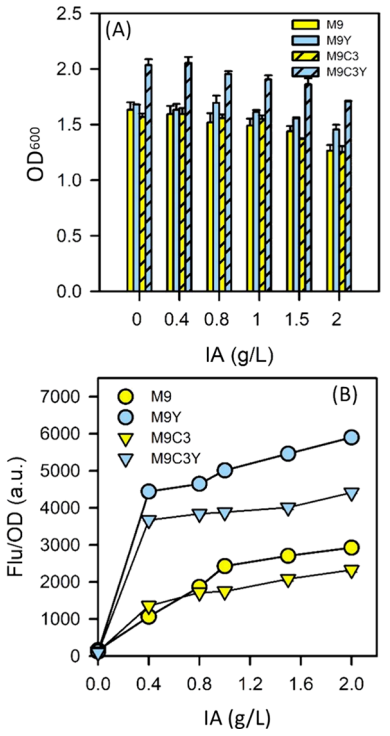


**Figure 2.** IA biosensor in M9, M9Y, M9C3, and M9C3Y media under different IA concentrations ranging from 0 to 2 g/L. (A) Biomass and (B) specific fluorescence signal in four media.

of 2547 and 3347 a.u., respectively (Figure S1). The dynamic range was 1.82-folds in M9 and 1.33-folds in M9Y, when the IA concentration increased from 0.4 to 2 g/L. Therefore, the higher dynamic range within low concentration was observed in M9Y, while the higher dynamic range within higher concentration was observed in M9. Considering the higher fluorescence intensity signal, M9Y was chosen as the preferable screening medium.

**Intracellular Synchronic Sensing and IA Production.** IA is a natural product in several bacteria, such as *A. rerreus*, *U. maydis*, and *U. cynodontis* except for *E. coli*.[36] Fortunately, citrate, the precursor of IA, is natively metabolized in the TCA cycle of *E. coli* with reversible isomerization from citrate to isocitrate facilitated by aconitate hydratase B (encoded by *acn*B) (Figure 3A). Consequently, the regulation of the metabolic flux is crucial for IA production. Herein, five deletion strains from KEIO collection including *ace*A, *pta*, *ack*A, *icl*R, and *icd*[37] were selected to evaluate intrinsic IA production based on the fluorescence of the biosensor. The lowest biomass in terms of $OD_{600}$ was observed in the BWΔ*ack*A, which led to the highest specific fluorescence. The total fluorescence was higher in BWΔ*icl*R and BWΔ*icd* strains, and negligible IA production was detected in the BWΔ*icd* strain (Table S1). To facilitate IA production, a recombinant plasmid for AtCadA overexpression was introduced into different deletion hosts promoting the conversion of cis-aconitate to IA. Based on the biosensor output, the specific fluorescence at 36 h was 1257, 1217, 1068, 907, and 455 a.u. for BWΔ*icd*, BWΔ*icl*R, BWΔ*pta*, BWΔ*ack*A, and BWΔ*ace*A, respectively (Figure 3B). Correspondingly, the IA production was consistent with the specific fluorescence reaching 0.54, 0.48, 0.30, 0.25, and 0.15 g/L in BWΔ*icd*, BWΔ*icl*R, BWΔ*pta*, BWΔ*ack*A, and BWΔ*ace*A strains, respectively, at 36 h (Figure 3C). Several genes influenced the production of byproducts


https://doi.org/10.1021/acssynbio.3c00344
ACS Synth. Biol. 2023, 12, 3020−3029

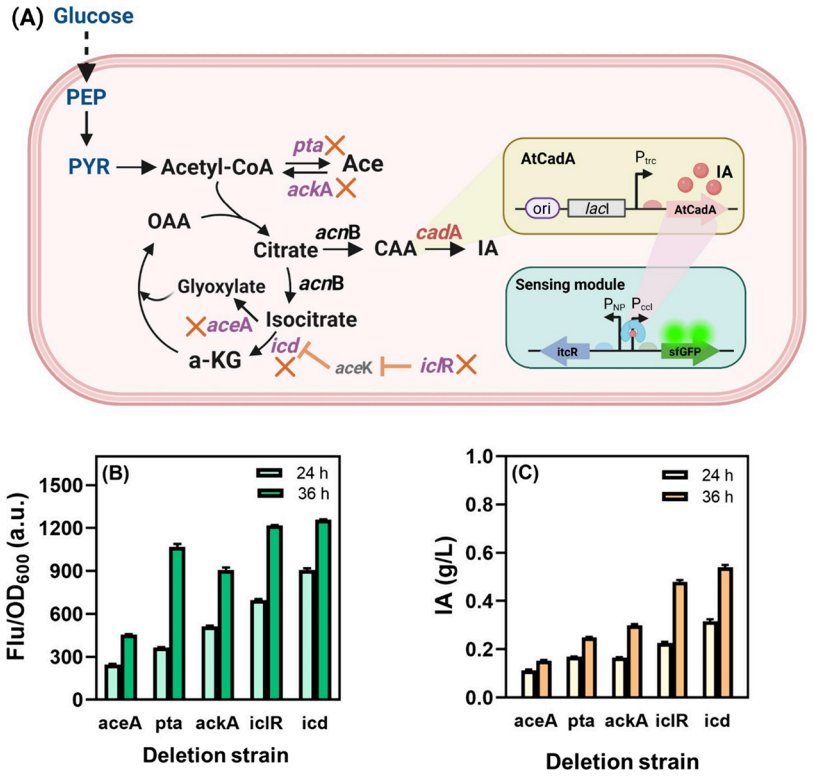


**Figure 3.** Intracellular itaconic acid production in different deletion strains to select screening host for AtCadA mutation. (A) Illustration of intracellular itaconic acid production from the metabolic pathway in *E. coli*. The five individual gene deletion strains were indicated by the cross symbol. (B) Specific fluorescence and (C) IA production of five deletion strains harboring biosensor plasmid pSCA-itcR-$P_{ccl}$-sfGFP and recombinant plasmid pSUI-trc-AtCadA at 24 and 36 h, respectively. Abbreviations list: phosphoenolpyruvate (PEP), pyruvate (PYR), acetate (Ace), *cis*-aconitic acid (CAA), itaconic acid (IA), alpha-ketoglutarate (a-KG), oxaloacetate (OAA), isocitrate lyase (aceA), phosphotransacetylase (pta), acetate kinase (ackA), transcriptional repressor (iclR), and isocitrate dehydrogenase (icd).

during IA synthesis including glyoxylate shunt and TCA cycle. Acetate, the major metabolite in cellular carbohydrate metabolism, is catabolized by the *pta* gene, which encodes phosphate acetyltransferase using acetyl-CoA as precursor. However, the formation of acetate reduces the ATP pool and decreases the level of pyruvate accumulation, thus affecting IA production. Notably, the disruption of *pta* and *ldh*A resulted in an improved IA production of 690 mg/L.[38,39] In glyoxylate shunt, the transcriptional regulator IclR governs the expression of *ace*BAK. Deletion of *icl*R strengthens the inhibition of *icd* gene by *ace*K, improving the levels of precursor isocitrate and replenishing the TCA cycle intermediates for IA production.[40,41] A 3.92-fold increase in IA production was reported following *icl*R deletion in the acid-resistant W strain.[42] On the other hand, the deletion or down-regulation of *icd* gene was crucial for IA production that resulted in the accumulation of isocitrate.[43] In accordance with the lowest basal IA production, strain BWΔ*ace*A was identified as the optimal screening host for AtCadA evolution.

**Engineered T7 Promoter for Altering the Mutation Efficiency.** *In vivo* target specific mutagenesis facilitated by deaminase-based T7RNAP involves modification of the DNA sequence during transcription by an altered deaminase[16] when the distinct domain of promoter DNA is recognized by the RNAP. The sequence of T7 promoter includes a binding domain spanning from −17 to −5 base pairs and a melting domain ranging from −4 to −1 base pairs,[44] which interacts with a specific loop (residue 742 to residue 773) in T7RNAP to form a T7RNAP-DNA complex.[45] A previous study revealed that mutations in the binding domain of T7RNAP influenced the binding affinity between T7RNAP and the T7 promoter.[46,47] Rather than modifying T7RNAP itself, we theorized that alterations in the base pair within the T7 promoter sequence could regulate the transcriptional efficiency of T7RNAP, subsequently resulting in different mutation rates. The T7 promoter region is divided into three parts, including (i) an upstream region (−12 to −17, U) and (ii) a central region (−7 to −11, C) for polymerase binding and (iii) a downstream region (−1 to −6, D) for transcription initiation. Each part was redesigned with a 4-mer random codon to establish a mutant library (Figure 4A). For screening using sfGFP, the expression level was detected in three categories for each design based on the fluorescence intensity of sfGFP as follows: strong (S) − fluorescence intensity above 15000 a.u., medium (M) − fluorescence intensity between 5000 and 15000 a.u., and weak (W) − fluorescence intensity below 5000 a.u. Compared to the control with the original T7 promoter, the average specific fluorescence was 18300 a.u. in the strong group, 12800 a.u. in the medium group, and 3900 a.u. in the weak group (Figure 4B). Sequence analysis revealed that AT-rich codons in the upstream and downstream regions (i.e., US and DS) were associated with strong fluorescence, while GC-codons were prevalent in the central region (i.e., CS). On the other hand, no codon preference was observed for medium and weak fluorescence (Table 1). It was reported that base pair changes at positions −11, −12, and −13 decreased the overall binding affinity of T7RNAP toward the T7 promoter,[44] which is within the central region, potentially explaining the


https://doi.org/10.1021/acssynbio.3c00344
ACS Synth. Biol. 2023, 12, 3020−3029

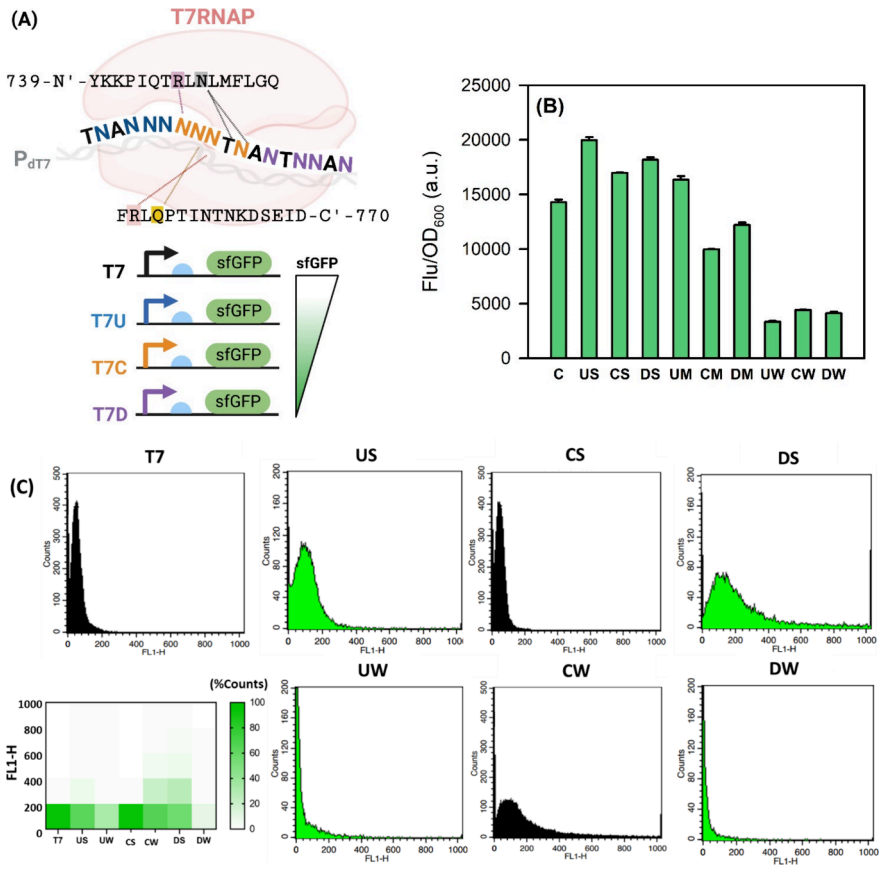


**Figure 4.** Engineered T7 promoter for altering the binding affinity of T7RNAP. (A) Schematic diagram of the dT7 promoter design using degenerated codons in the upstream, central, and downstream regions within the T7 promoter (i.e., T7U, T7C, and T7D, respectively). The interaction between the T7RNAP and T7 promoter are illustrated in pink, orange, and gray colors. (B) Specific fluorescence intensity of 10 different colonies from 9 degenerated pools and 1 control at 12 h. (C) FACS analysis after the mutation by MutaT7 with T7RNAP binding on T7, US, UW, CS, CW, DS, and DW.

**Table 1. Sequence Profile of the dT7 Promoter from Strong (S), Medium (M), and Weak (W) with Degenerated Codon in the Upstream (U), Central (C), and Downstream (D) Position**

| dT7 promoter | Sequencing profile from 3' to 5' | T7 sequence |
|---|---|---|
| US | 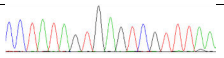 | TTAAACGACTCACTATAG |
| CS | 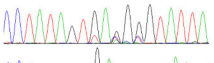 | TAATACCCCTCACTATAG |
| DS | 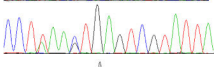 | TAATACGACTCAGTTAAG |
| UM | 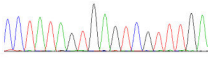 | TCAAACGACTCACTATAG |
| CM | 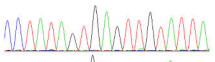 | TAATACAACTCACTATAG |
| DM | 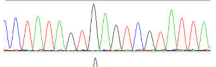 | TAATACGACTCACTATAG |
| UW | 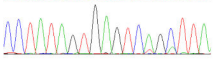 | TAAGCTGACTCACTATAG |
| CW | 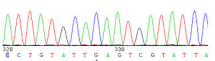 | TAATACGTGTTACTATAG |
| DW | 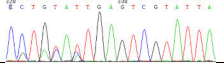 | TAATACGACTCAATACAG |

decreased fluorescence in CW. To verify the effect of promoter strength on the mutation efficiency, the expression levels of sfGFP under different promoter variants with MutaT7 was examined. The fluorescence distribution from each mutant was screened by using flow cytometry. As shown in Figure 4C, a broader fluorescence distribution was observed in CW and DS promoters, which possessed higher fluorescent colony counts in the range of 600 to 1000 a.u. (2.18% count for CW and 3.61% count for DS). In contrast, other variants maintained the fluorescence within 0 to 200 a.u., similar to the profile of the original T7 promoter. Notably, apart from the upstream region of the transcription site (+1), Conrad et al. illustrated that bases at the position +4 to +8 were also crucial in altering the activity of T7 promoter.[46] Additionally, the three-way junction of split T7 promoter, target RNA and T7RNAP has been utilized for specific viral RNA detection.[48] As a result, it is suggested that variations in T7 promoter strength alter the transcription rate, further tuning the mutation efficiency of deaminase-fused T7RNAP.

**Application of the Reverse T7 Promoter for Directed Evolution of AtCadA.** Enhancing the heterologous production of IA in various microorganisms relies on the overexpression of CadA. However, inefficient soluble protein production and feedback inhibition of CadA resulted in low IA titer.[49] To address these problems, directed evolution of AtCadA was performed by *in vivo* target-specific mutagenesis using MutaT7, followed by screening from the transcription-based biosensor to differentiate the superior variants (Figure 5A). Considering the fact that the plasmid copy number (PCN) could affect gene expression in the case of dual


https://doi.org/10.1021/acssynbio.3c00344
ACS Synth. Biol. 2023, 12, 3020−3029

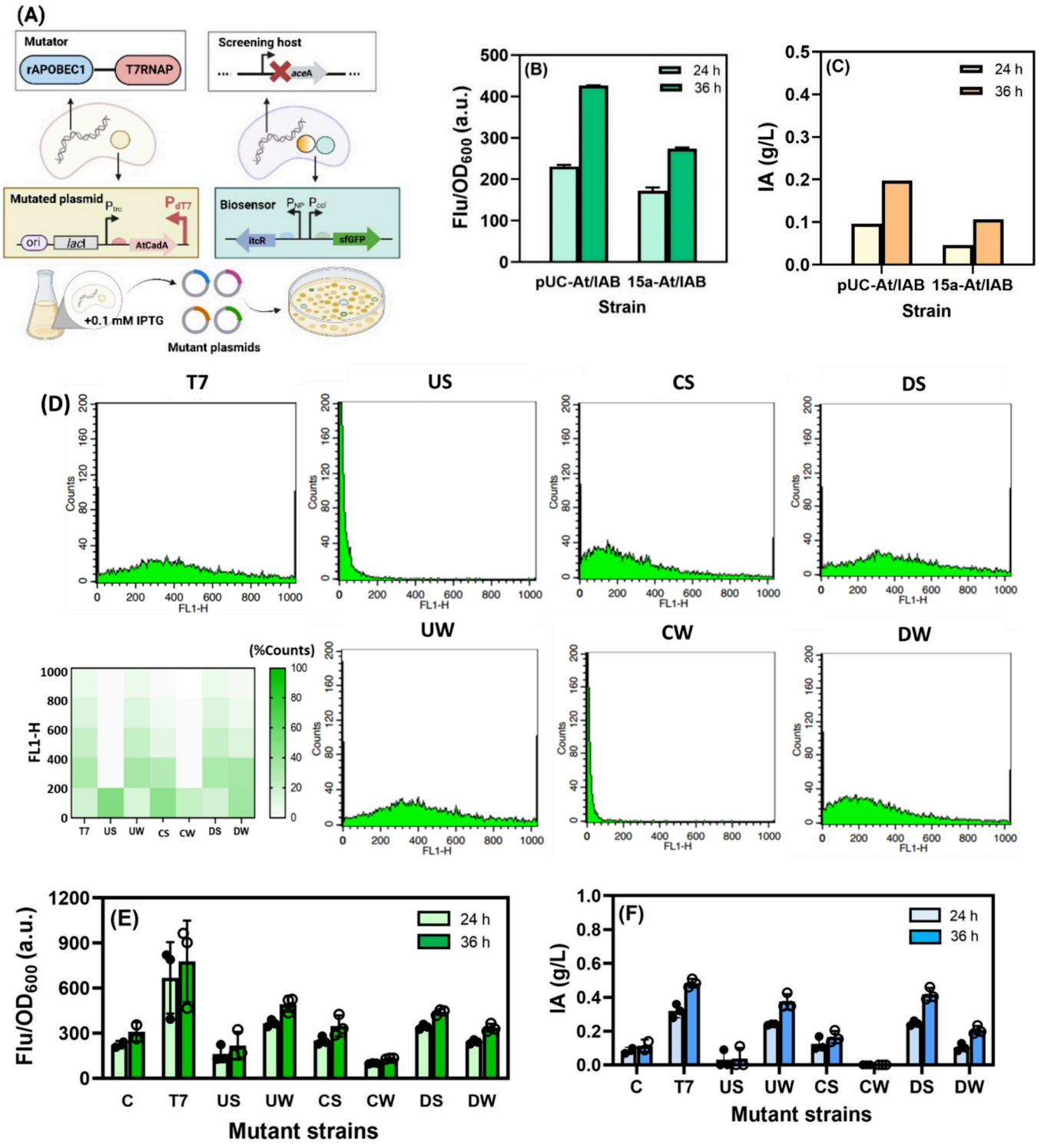


**Figure 5.** Directed evolution of AtCadA by MutaT7 and screened by the itaconic acid biosensor. (A) Illustration of the mutation by MutaT7 harboring the mutation plasmids and screened by the itaconic acid biosensor in BWΔaceA strain. The mutation process was conducted under 0.1 mM IPTG induction for 24 h. (B) Specific fluorescence and (C) IA production of two strains (pUC-At/IAB and 15a-At/IAB) harboring plasmids with different replication origins for mutation at 24 and 36 h, respectively. (D) FACS analysis of the pool of AtCadA mutants after the mutation by MutaT7 with T7RNAP binding on T7, US, UW, CS, CW, DS, and DW. The fluorescence signal was from the activator-based biosensor at 36 h. (E) Specific fluorescence and (F) IA production of seven mutants from different T7 promoters with orthogonality on MutaT7 at 24 and 36 h, respectively. The "C" control is without mutation.

plasmids, the effect of replication origin (ori) on fluorescence and IA production was investigated using the pUC or 15a vector for AtCadA (i.e., pUC-At or 15a-At). As shown in Figure 5B, specific fluorescence was about 410 a.u. in the strain harboring pUC-At/IAB with 0.22 g/L IA production at 36 h. The remarkable performance of a high-copy plasmid illustrated the consistent relationship between intracellular IA and fluorescence (Figure 5C). The PCN was determined based



https://doi.org/10.1021/acssynbio.3c00344
ACS Synth. Biol. 2023, 12, 3020−3029

on the replication origin of IAB biosensor using pSC101 and AtCadA with pUC or p15a backbones. As shown in Table 2,

**Table 2. Plasmid copy numbers (PCN) of the biosensor (IAB), and mutation plasmids of pUC-At and 15a-At[a]**

| | replication origin (PCN) | | |
|---|---|---|---|
| strains | pSC101 | pUC | p15A |
| IAB | 67.9 | | |
| pUC-At/IAB | 90.8 | 412.4 | |
| 15a-At/IAB | 65.3 | | 32.4 |

[a]IAB indicates the strains harboring only IA biosensor plasmid.

the PCN of a single IAB plasmid was 67.9, while this increased to 90.8 in the dual plasmid system pUC-At/IAB. On the other hand, the PCN of pUC was 412.4, indicating an imbalance in PCN when combining pUC-At and IAB, with a 4.5-fold difference between the two plasmids. Therefore, owing to the balanced PCN observed in the strain harboring 15a-At/IAB (i.e., 32.4 for 15a and 65.3 for pUC), the 15a backbone was selected for the expression of AtCadA.

To evaluate variations in mutation efficiency based on fluorescence and IA titers, 7 reverse dT7 promoters were constructed downstream of AtCadA. Fluorescence distribution of mutant plasmids from different promoters was again examined using FACS analysis. As shown in Figure 5D, a broad fluorescence distribution was observed in T7, UW, and DS, displaying a higher fluorescence colony count in the range of 600 to 1000 a.u. (19.59% for T7, 18.83% for UW, and 19.58% for DS). Conversely, the fluorescence distribution of CS and DW was in the range of 0 to 400 a.u., while that of US and CW was below 200 a.u., indicating weak or no fluorescent colonies. To further validate the mutants, IA production and synchronic sensing were conducted (Figure 5E,F), aligning with FACS sorting results. Variants derived from T7, UW, and DS showed elevated fluorescence and IA production compared to others, with the highest average fluorescence (860 a.u.) and IA (0.51 g/L) attained via *in vivo* mutagenesis of AtCadA using the T7 promoter. Jeon et al. constructed a library of synonymous codon library at the first 10 codons of AtCadA to overcome the problem of insoluble protein.[50] On the other hand, coexpression of chaperon proteins is another strategy for improving protein folding that increased IA production by 13%,[51] while another successful study used *E. coli* Lemo21-(DE3) in which T7RNAP is controlled by LysY.[52] However, the evolution of AtCadA has seldom addressed. Therefore, this study demonstrated a platform of the directed evolution of AtCadA for the first time. We observed the difference in fluorescence intensity and IA titer among different dT7 designs obtained from the mutant pool of multiple colonies.

## MATERIALS AND METHODS

**Chemical Reagents and Materials.** Luria−Bertani (LB) broth was purchased from Difco (Franklin Lakes, New Jersey). All the chemicals were purchased from Showa Chemical Industry Co., Ltd. (Saitama Prefecture, Japan) and Sigma-Aldrich (St. Louis, Missouri, USA) at analytic or HPLC grade. Enzymes used for DNA manipulation were purchased from New England Biolabs Ltd. (Massachusetts, US) and GeneDireX, Inc. (Taoyuan, Taiwan). Primers and gene synthesis were synthesized from Integrated DNA Technologies, Inc. (Coralville, US). DNA sequences were analyzed by Genomics (Keelung, Taiwan).

**Bacterial Strains and Cultural Medium.** Strains used in this study are given in Table 3. *E. coli* DH5$\alpha$ was used as cloning strain, while MutaT7 strain (Addgene #156460) was used for the *in vivo* gene mutation, and BWΔaceA strain (CGSC #10858) was used for mutant screening. Precultures were performed in Luria−Bertani (LB) medium (10 g/L NaCl, 10 g/L tryptone, and 5 g/L yeast extract) with the appropriate antibiotics (i.e., 100 $\mu$g/mL of Amp, 50 $\mu$g/mL of Kan, 25 $\mu$g/mL of *Cm* or 50 $\mu$g/mL of Strep). For the protein expression,

**Table 3. Strains and Plasmids Used in This Study**

| strains | description | remark |
|---|---|---|
| DH5$\alpha$ | F$^-$ endA1 gln *V*44 thi$^{-1}$ recA1 relA1 gyrA96 deoR nupG Φ80d *lacZ*ΔM15 Δ(*lacZYA-argF*) U169, hsdR17($r_K^-$ $m_K^+$), $\lambda^-$ | lab stock |
| BL21(DE3) | F$^-$ *ompT gal dcm lon hsd*$S_B$($r_B^-$ $m_B^-$) $\lambda$(DE3 [lacI lacUV5-T7p07 ind1 sam7 nin5]) [malB+]$_{K\text{-}12}$($\lambda^S$) | NEB #C2527I |
| JW2293−1 | F-, Δ(araD-araB)567, ΔlacZ4787(::rrnB-3), λ-, ΔackA778::kan, rph-1, Δ(rhaD-rhaB)568, hsdR514 | CGSC#9843 |
| JW2294−1 | F-, Δ(araD-araB)567, ΔlacZ4787(::rrnB-3), λ-, Δpta-779::kan, rph-1, Δ(rhaD-rhaB)568, hsdR514 | CGSC#9844 |
| JW1122−2 | F-, Δ(araD-araB)567, ΔlacZ4787(::rrnB-3), λ-, Δicd-724::kan, rph-1, Δ(rhaD-rhaB)568, hsdR514 | CGSC#9051 |
| JW3975−3 | F-, Δ(araD-araB)567, ΔlacZ4787(::rrnB-3), λ-, rph-1, Δ(rhaD-rhaB)568, ΔaceA782::kan, hsdR514 | CGSC#10858 |
| JW3978−2 | F-, Δ(araD-araB)567, ΔlacZ4787(::rrnB-3), λ-, rph-1, Δ(rhaD-rhaB)568, ΔiclR785::kan, hsdR514 | CGSC#10861 |
| MutaT7 | DH10B Δung ΔmotAB ΔcsgABCDEFG [PlacI-Ptac] Δ(araA-leu)7697::[PA1lacO-Tenth MutaT7] | Addgene #156460 |
| Plasmids | | |
| pSCA-J23100-sfGFP | 4293 bp, Amp$^R$, pSC101 ori, J23100 promoter, B0034 RBS, *sfgfp* | lab stock |
| pSCA-itcR-$P_{ccl}$-sfGFP | 5264 bp, Amp$^R$, pSC101 ori, native promoter and RBS, *itc*R, Pccl, *sfgfp* | this study |
| pSCA-itcR-$P_{ccl}$-RCP | 5264 bp, Amp$^R$, pSC101 ori, native promoter and RBS, *itc*R, Pccl, *rfp* | this study |
| pSCA-itcR-$P_{ccl}$-OFP | 5264 bp, Amp$^R$, pSC101 ori, native promoter and RBS, *itc*R, Pccl, *ofp* | this study |
| pSCA-itcR-JB34-$P_{ccl}$-sfGFP | 5329 bp, Amp$^R$, pSC101 ori, native promoter and RBS, J23100, B0034, *itc*R, Pccl, *sfgfp* | this study |
| pSCA-itcROP-JB34-$P_{ccl}$-sfGFP | 5329 bp, Amp$^R$, pSC101 ori, native promoter and RBS, J23100, B0034, optimized *itc*R, Pccl, *sfgfp* | this study |
| pET28a-sfGFP | 6013 bp, Kan$^R$, pBR322 ori, *lac*I, $P_{T7}$ promoter, *sfgfp* | 53 |
| pSUI-trc-AtCadA | 5091 bp, *Cm*$^R$, pUC ori, $P_{trc}$ promoter, *Atcad*A | this study |
| pSAI-trc-AtCadA | 5264 bp, *Cm*$^R$, p15a ori, $P_{trc}$ promoter, *Atcad*A | this study |
| pSAI-trc-AtCadA-T7 | 5283 bp, *Cm*$^R$, p15a ori, $P_{trc}$ promoter, *Atcad*A, original T7 promoter | this study |
| pSAI-trc-AtCadA-dT7 | 5283 bp, *Cm*$^R$, p15a ori, $P_{trc}$ promoter, *Atcad*A, degenerated dT7 promoter | this study |


https://doi.org/10.1021/acssynbio.3c00344
ACS Synth. Biol. 2023, 12, 3020−3029

2% (*v*/*v*) cells were inoculated into 10 mL of LB medium and cultured at 37 °C with shaking at 200 rpm. For intracellular IA production, M9 medium (6.35 g/L $Na_2HPO_4$, 1.5 g/L $KH_2PO_4$, 10 g/L glucose, 3 mM $MgSO_4$, 1 mM $CaCl_2$−$H_2O$) or M9C3 with 10 g/L glycerol to replace glucose, modified M9Y, or M9C3Y with 0.5 g/L yeast extract was used. The cells were cultivated in 30 mL of M9Y medium at 30 °C with shaking at 180 rpm until 48 h. The cell growth, fluorescence intensity, and IA production were monitored at 24, 36, and 48 h.

**Plasmid Construction for Sensing IA.** An initial itaconic acid biosensor plasmid pSCA-itcR-$P_{ccl}$-sfGFP containing the regulator ItcR and its cognate promoter $P_{ccl}$ from *Y. pseudotuberculosis* was synthesized by IDT. The biosensor cassette was amplified with $itcR_{fwd}$/$P_{ccl\ rev}$, and the *Xba*I/*Hin*dIII-digested fragment was introduced upstream of *sf*GFP of plasmid pSCA-J23100-sfGFP. For other fluorescence reporters, the *sfgfp* was replaced with an orange fluorescence reporter (OFP) or red chromoprotein (RCP) by *Hin*dIII and *Pst*I digestion. To fine-tune the regulator amount, the codon-optimized itcR (itcROP), additional promoter J23100 and RBS B0034, and its cognate promoter $P_{ccl}$ were synthesized by IDT and were amplified by J100-$P_{ccl\ fwd}$/B034-$itcR_{rev}$, and cloned into pSCA-J23100-sfGFP, generating pSCA-itcROP-JB34-$P_{ccl}$-sfGFP. The pSCA-itcR-JB34-$P_{ccl}$-sfGFP was constructed by replacing the itcROP with itcR, which was amplified by $itcR_{fwd}$ and $itcR_{rev}$.

**Plasmid Construction for Evolved MutaT7.** The degenerated codon was designed upstream, central, and downstream of the T7 promoter, which was constructed by oligo annealing using primers with overhang (i.e., Bl-dT7U-$X_{fwd}$ and X-dT7U-$Bl_{rev}$ for upstream design, Bl-dT7C-$X_{fwd}$ and X-dT7C-$Bl_{rev}$ for middle design, and Bl-dT7D-$X_{fwd}$ and X-dT7D-$Bl_{rev}$ for the downstream design). The degenerated promoter fragments were cloned into pET28a-sfGFP,[53] which was digested with *Bgl*II and *Xba*I. For the mutation plasmids, two variants of the dT7 promoter from each design were denoted as strong and weak promoters (e.g., US, UW indicated strong and weak promoter from the upstream design). First, the low copy plasmid pSAI-trc-sfGFP was constructed by replacing the pUC ori fragment in pSUI-trc-sfGFP with *Sac*I/*Pst*I-digested fragments. To construct different reverse dT7 promoters downstream of AtCadA, the target fragments were amplified by *Bam*HI-RBS-*Hin*dIII-$At_{fwd}$ and *Pst*I-dT7 series-$At_{rev}$. The *Bam*HI/*Pst*I-digested fragments replaced the *sfgfp* fragment in the backbone of pSAI-trc-sfGFP generating plasmids of the pSAI-trc-At-dT7 series. The constructive plasmids were further sequenced commercially. All primers are shown in Table S2.

**Characterization of Itaconic Acid Biosensor.** *E. coli* DH5*α* cells harboring pSCA-itcR-$P_{ccl}$-sfGFP or its derivatives were grown in itaconic acid-free medium, supplemented with different concentrations of itaconic acid (0, 0.4, 0.8, 1.0, 1.5, and 2 g/L). The fluorescence intensity was measured in 96-well microtiter plate using Microplate Readers SpectraMax M2 (Molecular Devices, CA). The wavelength (nm) of excitation and emission for sfGFP, OFP, and RCP was 480/510, 500/570, and 600/650, respectively. For the medium effect of biosensor, cells harboring pSCA-itcR-$P_{ccl}$-sfGFP was cultivated at M9 or M9Y medium with different IA values (0, 0.05, 0.1, 0.2, 0.25, 0.4, 0.8, 1.0, 1.5, and 2 g/L), while IA concentrations were used 0.4, 0.8, 1.0, 1.5, and 2 g/L in M9C3 and M9C3Y medium. The optical density of cells was monitored at a wavelength of 600 nm using Microplate Readers SpectraMax M2 (Molecular Devices, CA). The specific fluorescence Flu/OD was calculated from the ratio of fluorescence and the optical density. The slope of the calibration curve for the biosensor was simulated using linear regression. The dynamic range was defined using the fluorescence ratio between the highest and lowest IA titer.

**Directed Evolution of Target Protein by MutaT7.** The target plasmids pET28a-dT7-sfGFP and pSAI-trc-At-dT7 were transformed into MutaT7, respectively. A single colony was precultured in LB medium with appropriate antibiotics at 37 °C while being shaken at 200 rpm overnight. Next, 2% of cells were inoculated in LB medium with 0.1 mM IPTG supplemented initially and incubated at 37 °C with shaking at 200 rpm for 24 h to perform the directed evolution. The mutated plasmids were extracted for further screening.

**Biosensor-Based Screening.** A 300 ng amount of each plasmid biosensor pSCA-itcR-$P_{ccl}$-sfGFP and mutation plasmid pSAI-trc-At*-dT7 (or the control pSAI-trc-At) was cotransformed into the screening strain BWΔaceA. After recovery, the cells were grown on LB agar plates at 30 °C for 24 h. The variants were observed from the fluorescence difference on the plates and randomly selected several colonies to cultivate in M9Y medium for further evaluation by fluorescence intensity and itaconic acid titer.

**Fluorescence-Activated Cell Sorting (FACS) Analysis.** FACS analysis and data collection were conducted by a FACS Calibur (BD Biosciences, USA). A sample of cells with pET28a-dT7-sfGFP or dual plasmids pSAI-trc-At*-dT7 and pSCA-itcR-$P_{ccl}$-sfGFP after mutation from MutaT7 was diluted in ice-cold phosphate buffered saline (PBS, 37 mM NaCl, 2.7 mM KCl, 10 mM $Na_2HPO_4$, 1.8 mM $KH_2PO_4$, pH 7.4) to an optical density of <1.0 and analyzed according to the scatter characteristics (forward and side scatter). A 488 nm laser was applied to detect the fluorescence signal of sfGFP which excited at 488 nm and emitted at a bandpass filter at 530/30 nm. Total events were set at 10000. The mutation efficiency was depending on the events in each fluorescence range divided by the total events.

**HPLC Analysis.** The metabolites including glucose, itaconic acid, and acetate were analyzed by HPLC (Hitachi, Japan). The filtered supernatant from culture broth was injected to the column 87H3 (Transgenomic, USA) at 70 °C, using 8 mM $H_2SO_4$ as the mobile phase at 0.4 mL/min flow rate under refractive index (RI) detection at 210 nm.

## ■ ASSOCIATED CONTENT

### Data Availability Statement

Data will be made available on reasonable request.

### Supporting Information

The Supporting Information is available free of charge at https://pubs.acs.org/doi/10.1021/acssynbio.3c00344.

(Table S1) Biomass and specific fluorescence in deletion strains; (Table S2) primers used in this study; (Figure S1) calibration curve of IA biosensor (PDF)

## ■ AUTHOR INFORMATION

### Corresponding Author

**I-Son Ng** − *Department of Chemical Engineering, National Cheng Kung University, Tainan 70101, Taiwan*; Email: yswu@mail.ncku.edu.tw



https://doi.org/10.1021/acssynbio.3c00344
*ACS Synth. Biol.* 2023, 12, 3020−3029

## Author

**Wan-Wen Ting** − *Department of Chemical Engineering, National Cheng Kung University, Tainan 70101, Taiwan;* orcid.org/0000-0002-3018-4774

Complete contact information is available at: https://pubs.acs.org/10.1021/acssynbio.3c00344


## Author Contributions

W.W.T. and I.S.N. conceived the study. W.W.T. performed all the experiments and sketched the original draft. I.S.N. did methodology validation, supervised the experiments, reviewed, and edited the manuscript.


## Funding

The authors are grateful for the financial support for this study provided by the Ministry of Science and Technology (MOST 110−2221-E-006−030-MY3 and MOST 111−2221-E-006−012-MY3, NSTC 112−2218-E-006−022) in Taiwan.


## Notes

The authors declare no competing financial interest.
All the authors have read and agreed the ethics for publishing the manuscript.

## REFERENCES


(1) Brooks, S. M.; Alper, H. S. Applications, challenges, and needs for employing synthetic biology beyond the lab. *Nat. Commun.* **2021**, *12* (1), 1390.
(2) McCarty, N. S.; Ledesma-Amaro, R. Synthetic biology tools to engineer microbial communities for biotechnology. *Trends Biotechnol.* **2019**, *37* (2), 181−197.
(3) Schmidt-Dannert, C.; Lopez-Gallego, F. A roadmap for biocatalysis−functional and spatial orchestration of enzyme cascades. *Microb. Biotechnol.* **2016**, *9* (5), 601−609.
(4) Sharma, A.; Gupta, G.; Ahmad, T.; Mansoor, S.; Kaur, B. Enzyme engineering: current trends and future perspectives. *Food Rev. Int.* **2021**, *37* (2), 121−154.
(5) Zhao, H.; Giver, L.; Shao, Z.; Affholter, J. A.; Arnold, F. H. Molecular evolution by staggered extension process (StEP) in vitro recombination. *Nat. Biotechnol.* **1998**, *16* (3), 258−261.
(6) Arnold, F. H. Directed evolution: bringing new chemistry to life. *Angew. Chem., Int. Ed.* **2018**, *57* (16), 4143−4148.
(7) Wang, Y.; Xue, P.; Cao, M.; Yu, T.; Lane, S. T.; Zhao, H. Directed evolution: methodologies and applications. *Chem. Rev.* **2021**, *121* (20), 12384−12444.
(8) Porter, J. L.; Rusli, R. A.; Ollis, D. L. Directed evolution of enzymes for industrial biocatalysis. *ChemBioChem.* **2016**, *17* (3), 197−203.
(9) Gargiulo, S.; Soumillion, P. Directed evolution for enzyme development in biocatalysis. *Curr. Opin. Chem. Eng.* **2021**, *61*, 107−113.
(10) Ogawa, Y.; Katsuyama, Y.; Ueno, K.; Ohnishi, Y. Switching the ligand specificity of the biosensor XylS from meta to para-toluic acid through directed evolution exploiting a dual selection system. *ACS Synth. Biol.* **2019**, *8* (12), 2679−2689.
(11) Chen, D.; Xu, S.; Li, S.; Tao, S.; Li, L.; Chen, S.; Wu, L. Directly evolved AlkS-based biosensor platform for monitoring and high-throughput screening of alkane production. *ACS Synth. Biol.* **2023**, *12* (3), 832−841.
(12) Ho, J. M. L.; Miller, C. A.; Smith, K. A.; Mattia, J. R.; Bennett, M. R. Improved pyrrolysine biosynthesis through phage assisted non-continuous directed evolution of the complete pathway. *Nat. Commun.* **2021**, *12* (1), 3914.
(13) Crook, N.; Abatemarco, J.; Sun, J.; Wagner, J. M.; Schmitz, A.; Alper, H. S. In vivo continuous evolution of genes and pathways in yeast. *Nat. Commun.* **2016**, *7* (1), 13051.
(14) Kumar, R.; DiMenna, L.; Chaudhuri, J.; Evans, T. Biological function of activation-induced cytidine deaminase (AID). *Biomed. J.* **2014**, *37* (5), 269.
(15) Salter, J. D.; Bennett, R. P.; Smith, H. C. The APOBEC protein family: united by structure, divergent in function. *Trends Biochem. Sci.* **2016**, *41* (7), 578−594.
(16) Moore, C. L.; Papa, L. J., III; Shoulders, M. D. A processive protein chimera introduces mutations across defined DNA regions in vivo. *J. Am. Chem. Soc.* **2018**, *140* (37), 11560−11564.
(17) Chen, H.; Liu, S.; Padula, S.; Lesman, D.; Griswold, K.; Lin, A.; Zhao, T.; Marshall, J. L.; Chen, F. Efficient, continuous mutagenesis in human cells using a pseudo-random DNA editor. *Nat. Biotechnol.* **2020**, *38* (2), 165−168.
(18) Park, H.; Kim, S. Gene-specific mutagenesis enables rapid continuous evolution of enzymes in vivo. *Nucleic Acids Res.* **2021**, *49* (6), No. e32.
(19) Wolf, J. tadA, an essential tRNA-specific adenosine deaminase from *Escherichia coli*. *EMBO J.* **2002**, *21* (14), 3841−3851.
(20) Richter, M. F.; Zhao, K. T.; Eton, E.; Lapinaite, A.; Newby, G. A.; Thuronyi, B. W.; et al. Phage-assisted evolution of an adenine base editor with improved Cas domain compatibility and activity. *Nat. Biotechnol.* **2020**, *38* (7), 883−891.
(21) Mengiste, A. A.; Wilson, R. H.; Weissman, R. F.; Papa III, L. J.; Hendel, S. J.; Moore, C. L.; Butty, V. L.; Shoulders, M. D. Expanded MutaT7 toolkit efficiently and simultaneously accesses all possible transition mutations in bacteria. *Nucleic Acids Res.* **2023**, *51* (6), No. e31.
(22) Seo, D.; Eom, G. E.; Kim, H. W.; Kim, S. A dual gene-specific mutator system installs all transition mutations at similar rates in vivo. *bioRxiv* **2022**, *2022*, 2022−06.
(23) Zhang, L.; Guo, W.; Lu, Y. Advances in cell-free biosensors: principle, mechanism, and applications. *Biotechnol. J.* **2020**, *15* (9), No. 2000187.
(24) Yang, D.; Park, S. Y.; Park, Y. S.; Eun, H.; Lee, S. Y. Metabolic engineering of *Escherichia coli* for natural product biosynthesis. *Trends Biotechnol.* **2020**, *38* (7), 745−765.
(25) Shen, X.; Wang, J.; Li, C.; Yuan, Q.; Yan, Y. Dynamic gene expression engineering as a tool in pathway engineering. *Curr. Opin. Biotechnol.* **2019**, *59*, 122−129.
(26) Hevekerl, A.; Kuenz, A.; Vorlop, K. D. Influence of the pH on the itaconic acid production with *Aspergillus terreus*. *Appl. Microbiol. Biotechnol.* **2014**, *98* (24), 10005−10012.
(27) Hsiang, C. C.; Diankristanti, P. A.; Tan, S. I.; Ke, Y. C.; Chen, Y. C.; Effendi, S. S. W.; Ng, I. S. Tailoring key enzymes for renewable and high-level itaconic acid production using genetic *Escherichia coli* via whole-cell bioconversion. *Enzyme Microbial Technol.* **2022**, *160*, No. 110087.
(28) Sasikaran, J.; Ziemski, M.; Zadora, P. K.; Fleig, A.; Berg, I. A. Bacterial itaconate degradation promotes pathogenicity. *Nat. Chem. Biol.* **2014**, *10* (5), 371−377.
(29) Oliver, P.; Peralta-Gil, M.; Tabche, M. L.; Merino, E. Molecular and structural considerations of TF-DNA binding for the generation of biologically meaningful and accurate phylogenetic footprinting analysis: the LysR-type transcriptional regulator family as a study model. *BMC Genomics* **2016**, *17* (1), 1−17.
(30) Ding, N.; Zhou, S.; Deng, Y. Transcription-factor-based biosensor engineering for applications in synthetic biology. *ACS Synth. Biol.* **2021**, *10* (5), 911−922.
(31) Mannan, A. A.; Liu, D.; Zhang, F.; Oyarzún, D. A. Fundamental design principles for transcription-factor-based metabolite biosensors. *ACS Synth. Biol.* **2017**, *6* (10), 1851−1859.
(32) Gong, X.; Zhang, R.; Wang, J.; Yan, Y. Engineering of a TrpR-based biosensor for altered dynamic range and ligand preference. *ACS Synth. Biol.* **2022**, *11* (6), 2175−2183.
(33) Gao, J.; Du, M.; Zhao, J.; Xu, N.; Du, H.; Ju, J.; Wei, L.; Liu, J. Design of a genetically encoded biosensor to establish a high-throughput screening platform for L-cysteine overproduction. *Metabolic Eng.* **2022**, *73*, 144−157.

(34) Xu, S.; Zhang, L.; Zhou, S.; Deng, Y. Biosensor-based multigene pathway optimization for enhancing the production of glycolate. *Appl. Environ. Microbiol.* **2021**, *87* (12), No. e00113-21.
(35) Ding, N.; Yuan, Z.; Zhang, X.; Chen, J.; Zhou, S.; Deng, Y. Programmable cross-ribosome-binding sites to fine-tune the dynamic range of transcription factor-based biosensor. *Nucleic Acids Res.* **2020**, *48* (18), 10602−10613.
(36) Nascimento, M. F.; Marques, N.; Correia, J.; Faria, N. T.; Mira, N. P.; Ferreira, F. C. Integrated perspective on microbe-based production of itaconic acid: From metabolic and strain engineering to upstream and downstream strategies. *Process Biochem.* **2022**, *117*, 53−67.
(37) Baba, T.; Ara, T.; Hasegawa, M.; Takai, Y.; Okumura, Y.; Baba, M.; Datsenko, K. A.; Tomita, M.; Wanner, B. L.; Mori, H. Construction of *Escherichia coli* K-12 in-frame, single-gene knockout mutants: the Keio collection. *Mol. Systems Biol.* **2006**, *2* (2006), No. 0008.
(38) Vuoristo, K. S.; Mars, A. E.; Sangra, J. V.; Springer, J.; Eggink, G.; Sanders, J. P. M.; Weusthuis, R. A. Metabolic engineering of itaconate production in *Escherichia coli*. *Appl. Microbiol. Biotechnol.* **2015**, *99*, 221−228.
(39) Harder, B. J.; Bettenbrock, K.; Klamt, S. Model-based metabolic engineering enables high yield itaconic acid production by *Escherichia coli*. *Metab. Eng.* **2016**, *38*, 29−37.
(40) Noh, M. H.; Lim, H. G.; Woo, S. H.; Song, J.; Jung, G. Y. Production of itaconic acid from acetate by engineering acid-tolerant *Escherichia coli* W. *Biotechnol. Bioeng.* **2018**, *115* (3), 729−738.
(41) Harder, B. J.; Bettenbrock, K.; Klamt, S. Temperature-dependent dynamic control of the TCA cycle increases volumetric productivity of itaconic acid production by *Escherichia coli*. *Biotechnol. Bioeng.* **2018**, *115* (1), 156−164.
(42) Sun, W.; Vila-Santa, A.; Liu, N.; Prozorov, T.; Xie, D.; Faria, N. T.; Ferreira, F. C.; Mira, N. P.; Shao, Z. Metabolic engineering of an acid-tolerant yeast strain *Pichia kudriavzevii* for itaconic acid production. *Metab. Eng. Commun.* **2020**, *10*, No. e00124.
(43) Chang, P.; Chen, G. S.; Chu, H. Y.; Lu, K. W.; Shen, C. R. Engineering efficient production of itaconic acid from diverse substrates in *Escherichia coli*. *J. Biotechnol.* **2017**, *249*, 73−81.
(44) Bandwar, R. P.; Jia, Y.; Stano, N. M.; Patel, S. S. Kinetic and thermodynamic basis of promoter strength: multiple steps of transcription initiation by T7 RNA polymerase are modulated by the promoter sequence. *Biochemistry* **2002**, *41* (11), 3586−3595.
(45) Rong, M.; He, B.; McAllister, W. T.; Durbin, R. K. Promoter specificity determinants of T7 RNA polymerase. *Proc. Natl. Acad. Sci. U. S. A.* **1998**, *95* (2), 515−519.
(46) Guillerez, J.; Lopez, P. J.; Proux, F.; Launay, H.; Dreyfus, M. A mutation in T7 RNA polymerase that facilitates promoter clearance. *Proc. Natl. Acad. Sci. U. S. A.* **2005**, *102* (17), 5958−5963.
(47) Conrad, T.; Plumbom, I.; Alcobendas, M.; Vidal, R.; Sauer, S. Maximizing transcription of nucleic acids with efficient T7 promoters. *Commun. Biol.* **2020**, *3* (1), 439.
(48) Yoon, T.; Shin, J.; Choi, H. J.; Park, K. S. Split T7 promoter-based isothermal transcription amplification for one-step fluorescence detection of SARS-CoV-2 and emerging variants. *Biosens. Bioelectron.* **2022**, *208*, No. 114221.
(49) Bafana, R.; Pandey, R. A. New approaches for itaconic acid production: bottlenecks and possible remedies. *Crit. Rev. Biotechnol.* **2018**, *38* (1), 68−82.
(50) Jeon, H. G.; Cheong, D. E.; Han, Y.; Song, J. J.; Choi, J. H. Itaconic acid production from glycerol using *Escherichia coli* harboring a random synonymous codon-substituted 5′-coding region variant of the cadA gene. *Biotechnol. Bioeng.* **2016**, *113* (7), 1504−1510.
(51) Hsiang, C. C.; Tan, S. I.; Chen, Y. C.; Ng, I. S. Genetic design of co-expressing a novel aconitase with cis-aconitate decarboxylase and chaperone GroELS for high-level itaconic acid production. *Process Biochem.* **2023**, *129*, 133−139.
(52) Diankristanti, P. A.; Effendi, S. S. W.; Hsiang, C. C.; Ng, I. S. High-level itaconic acid (IA) production using engineered *Escherichia coli* Lemo21(DE3) toward sustainable biorefinery. *Enzyme Microb. Technol.* **2023**, *167*, No. 110231.
(53) Ting, W. W.; Tan, S. I.; Ng, I. S. Development of chromosome-based T7 RNA polymerase and orthogonal T7 promoter circuit in *Escherichia coli* W3110 as a cell factory. *Bioresour. Bioprocess.* **2020**, *7*, 54.


https://doi.org/10.1021/acssynbio.3c00344
*ACS Synth. Biol.* 2023, 12, 3020−3029